nature structural & molecular biology

Crystal structure of human stearoyl–coenzyme A desaturase in complex with substrate

Hui Wang, Michael G Klein, Hua Zou, Weston Lane, Gyorgy Snell, Irena Levin, Ke Li & Bi-Ching Sang

Stearoyl–coenzyme A desaturase-1 (SCD1) has an important role in lipid metabolism, and SCD1 inhibitors are potential therapeutic agents for the treatment of metabolic diseases and cancers. Here we report the 3.25-Å crystal structure of human SCD1 in complex with its substrate, stearoyl–coenzyme A, which defines the new SCD1 dimetal catalytic center and reveals the determinants of substrate binding to provide insights into the catalytic mechanism of desaturation of the stearoyl moiety. The structure also provides a mechanism for localization of SCD1 in the endoplasmic reticulum: human SCD1 folds around a tight hydrophobic core formed from four long α-helices that presumably function as an anchor spanning the endoplasmic reticulum membrane. Furthermore, our results provide a framework for the rational design of pharmacological inhibitors targeting the SCD1 enzyme.

© 2015 Nature America, Inc. All rights reserved.

Monounsaturated fatty acids are precursors in the assembly of lipids such as cholesteryl esters, triglycerides and phospholipids[1]. SCD1, a fatty-acid desaturase in the endoplasmic reticulum (ER), functions to maintain the cellular balance of saturated and monounsaturated lipids. SCD1 introduces a *cis* double bond at the Δ9 position (the bond between carbons 9 and 10) of the fatty acid in stearoyl–coenzyme A (CoA) or palmitoyl-CoA by coupling the electron-transport proteins NADH–cytochrome b_5 reductase and cytochrome b_5 (ref. 2). SCD1 belongs to the family of di-iron–containing desaturases, which consist of both soluble and membrane-bound forms. Structural studies on soluble desaturase acyl-acyl carrier proteins (acyl-ACPs)[3–6] have provided insight into the catalytic mechanisms of the soluble enzymes. However, direct structural information for integral membrane di-iron desaturase SCD1 has been elusive[7], although previous biochemical studies have guided initial topology predictions of mouse SCD1 (mSCD1)[8].

The dysregulation of SCD1 has been implicated in contributing to pathologies in diabetes[9], cancer[10] and many metabolic syndromes[11]. Cell-based and animal-tumor studies have shown that SCD1 plays a critical part in the regulation of lipid biosynthesis in cancer cells[12]. Furthermore, higher expression of SCD1 is associated with and higher plasma triglycerides[13] and increased insulin levels[14]. Thus, SCD1 inhibitors may serve as therapeutic agents to treat cancers and metabolic diseases, and this has inspired pharmaceutical research that has resulted in over 100 patent applications on SCD1 inhibitors in the past decade[15,16].

To provide a foundation for studying the molecular mechanisms of SCD1 function and to lay a framework for the rational design of SCD1 inhibitors, we determined the structure of human SCD1 (hSCD1) in complex with stearoyl-CoA substrate and two zinc ions. The substrate-bound hSCD1 structure reveals a new fold containing a unique histidine-coordinating dimetal catalytic center adjacent to a prominent kink in a long internal hydrophobic tunnel that holds the acyl chain of the substrate. Furthermore, we compared hSCD1 to other di-iron–containing enzymes and propose the determinants of regioselectivity and stereoselectivity in the dehydrogenation mechanism of SCD1.

RESULTS

We crystallized hSCD1 as a construct with the N-terminal 45 residues truncated and with three surface-exposed residues mutated (Online Methods). We determined the 3.25-Å crystal structure by SAD phasing, using crystals grown from native protein containing two intrinsic zinc atoms and from selenomethionine (SeMet)-labeled protein (Online Methods). The electron density maps from these two independent sources of phase information are well defined for the core of hSCD1. The final refined model contains residues 53–350 of hSCD1, a stearoyl-CoA molecule, two zinc ions, a detergent molecule and a water molecule (**Table 1**).

Architecture

hSCD1 folds into a mushroom-like architecture consisting of a stem of four transmembrane α-helices (TM stem) and a cytoplasmic domain (cap) (**Fig. 1a**,**b**). The four transmembrane helices (TM1–TM4) of the TM stem presumably span the ER membrane. The TM stem connects through two short ER-lumen loops (LL1 and LL2) and a long polypeptide linkage that extends into the cytoplasmic side of the ER. The topology of our hSCD1 crystal structure is consistent with previous predictions of mSCD1 topology[8]. The short lengths of LL1 and LL2 constrain the base of the TM stem. TM2 and TM4 are longer than TM1 and TM3, and their C-terminal ends interact with the cytoplasmic cap domain, which contains three histidines (His120, His125 and His269) that mediate metal binding. TM2 and TM4 also contain nonpolar residues that form a hydrophobic cavity for the acyl chain of the substrate (discussed below).

Department of Structural Biology, Takeda California, San Diego, California, USA. Correspondence should be addressed to H.W. (wanghui.takeda@gmail.com) or M.K. (michaelgklein@gmail.com).

Received 6 May; accepted 26 May; published online 22 June 2015; doi:10.1038/nsmb.3049

Table 1 Data collection and refinement statistics

	hSCD1	hSCD1 (SeMet)
Data collection		
Space group	$P3_121$	$P3_121$
Cell dimensions		
a, *b*, *c* (Å)	134.1, 134.1, 112.6	133.0, 133.0, 113.8
α, β, γ (°)	90.0, 90.0, 120.0	90.0, 90.0, 120.0
Resolution (Å)	40.0–3.25 (3.37–3.25)	50.3–3.60 (3.66–3.60)
R_{merge}	0.118	0.117
$I / \sigma I$	19.0 (1.0)	20.5 (1.6)
Completeness (%)	100 (100)	99.9 (100)
Redundancy	21.7 (21.2)	10.8 (6.2)
Refinement		
Resolution (Å)	37.5–3.25	
No. reflections	18,817	
R_{work} / R_{free}	0.241 / 0.263	
No. atoms		
Protein	2,466	
Ligand/ion	1 ST9, 2 Zn, 1 LMT	
Water	1	
B factors		
Protein	103.3	
Ligand/ion	102.9	
Water	104.2	
r.m.s. deviations		
Bond lengths (Å)	0.004	
Bond angles (°)	0.941	

Values in parentheses are for highest-resolution shell. ST9, stearoyl-CoA; LMT, *n*-dodecyl-D-maltopyranoside.

The cytoplasmic cap domain is formed by three segments of the SCD1 protein; the largest component is the long polypeptide between TM2 and TM3 (Ser127–Tyr217), which packs with two segments from the N terminus (Asp53–Val72) and from the C terminus (Phe271–Arg350). The cap domain is composed of ten cytoplasmic helices (CH1–CH10, numbered from N to C termini) and the connecting loops, many of which are solvent exposed (**Fig. 1**). The cap domain interlocks with the relatively splayed outside of the four–α-helix TM-stem domain. Residues in the cytoplasmic cap domain contribute to both metal binding and substrate recognition. The two buried zincs interact with segments from cytoplasmic-domain α-helices (CH2 and CH8) and the TM stem (TM2 and TM4). Sequence alignment between hSCD1 and mSCD1–4 and hSCD5 (**Supplementary Fig. 1**) reveals the very high degree of conservation in the SCD residues that participate in metal binding and in the residues that maintain the overall architecture of SCD1.

Metal-binding site

In the hSCD1 structure, we identified two metal-binding sites at the center of the cytoplasmic cap domain, on the basis of the unambiguous F_o–F_c omit electron density that we identified in maps generated from native protein crystals (**Fig. 2a**) and in anomalous difference Fourier density maps from both native protein crystals and SeMet-labeled protein crystals (**Fig. 2b**). The data sets used in structure determination contained strong anomalous signal, presumably from the metals (peaks of 23σ and 14σ for native and SeMet-labeled crystals, respectively). Although SCD1 is reportedly an iron-binding enzyme[8], we considered the possibility that the iron-binding sites in our SCD1 crystals could actually be occupied by alternative metals leached from the recombinant protein's expression medium. To determine the identity of the metal ions, we measured X-ray fluorescence and X-ray absorption from hSCD1 crystals (**Supplementary Fig. 2**). X-ray emission spectra collected at 15,000 eV and 11,000 eV (i.e., above the Zn K_{1s} edge of 9,659 eV) showed two strong peaks at 8,620 eV and 9,549 eV, corresponding to the Kα and Kβ X-ray emission lines of zinc. In contrast, a fluorescence spectrum collected below the Zn K_{1s} edge at 9,500 eV did not show these characteristic emission lines (**Supplementary Fig. 2a**,**b**). Furthermore, we confirmed the presence of zinc by an X-ray absorption scan across the Zn K_{1s} edge (**Supplementary Fig. 2c**). From these results, we assigned the two metals as zinc (Zn1 and Zn2).

Two zinc ions with a distance of 6.7 Å are coordinated through a network of residues that adopt a distorted trigonal bipyramidal geometry. In agreement with the predicted topology model of mSCD1 (ref. 8), the conserved histidines in the histidine-box motifs (HXXXXH, HXXHH and HXXHH) (ref. 17 and alignment in **Supplementary Fig. 1**) participate in the coordination of metal (**Fig. 2c**,**d**). Zn1 is coordinated by nitrogen atoms on the side chains of residues His120 (TM2), His125 (TM2), His157 (CH2), His161 (CH2) and His301 (CH8), and Zn2 is ligated with His160 (CH2), His269 (TM4), His298 (CH8) and His302 (CH8) (**Fig. 2c**,**d** and **Supplementary Fig. 3a**). The electron density in the vicinity of Zn2 is assigned to a water molecule, which is 2.1 Å away from the Zn2 center and 2.7 Å away from the carbonyl group of the carboxamide in Asn265 (TM4). The two zincs are within 4.5–5.5 Å of carbons 9 and 10 of stearoyl-CoA, thus defining the dehydrogenation catalytic center of SCD1 (**Fig. 2e**).

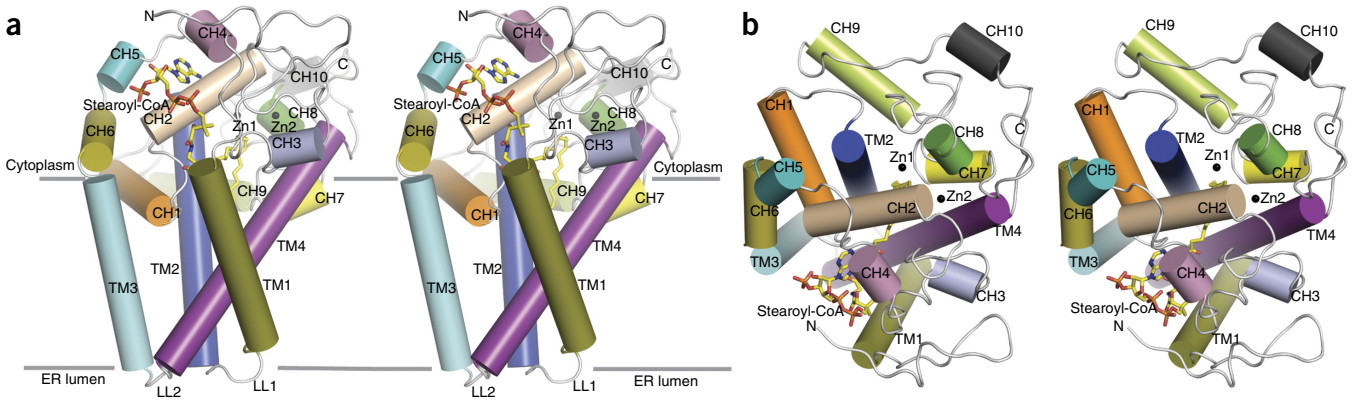

Figure 1 Overview of the hSCD1 structure. (**a**) Stereo view showing the orientation of SCD1 with respect to the plane of the membrane. The stearoyl-CoA is shown in stick representation and is colored yellow, and two zinc ions are shown as black spheres. (**b**) Stereo view of the SCD1 structure, highlighting the cytoplasmic-facing cap domain.

© 2015 Nature America, Inc. All rights reserved.

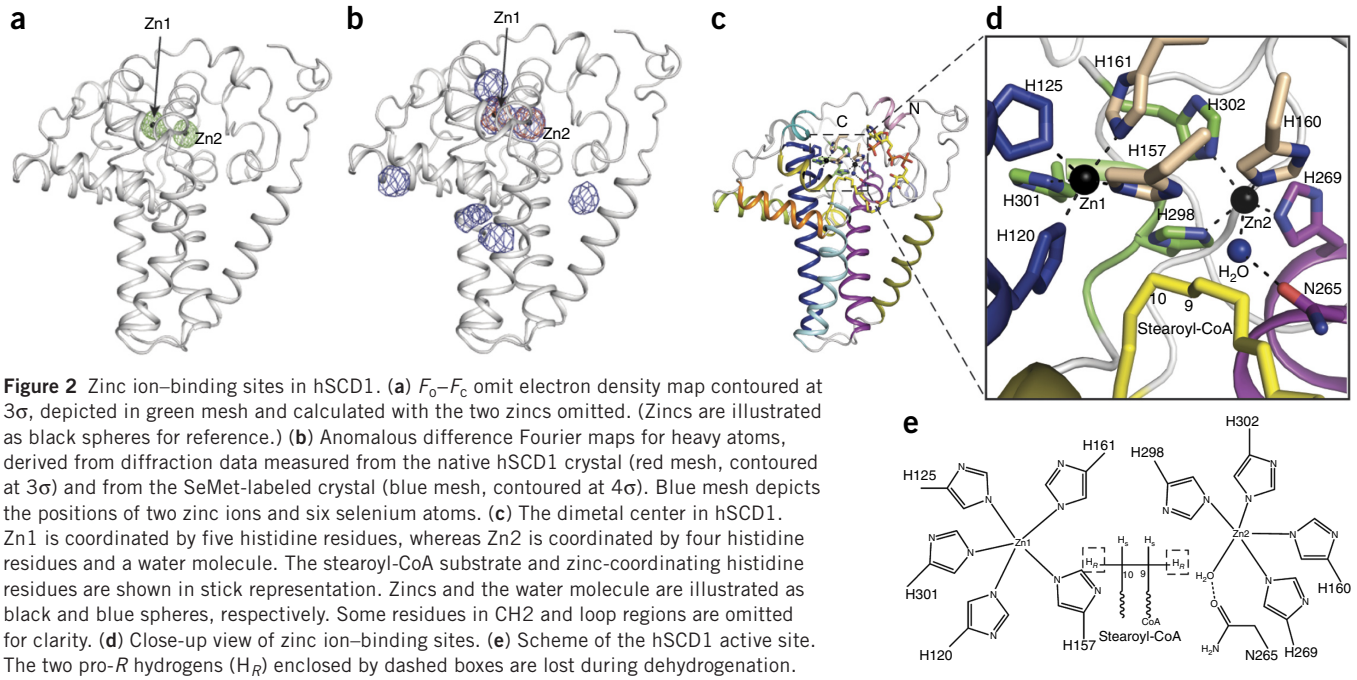

Figure 2 Zinc ion–binding sites in hSCD1. (**a**) F_o–F_c omit electron density map contoured at 3σ, depicted in green mesh and calculated with the two zincs omitted. (Zincs are illustrated as black spheres for reference.) (**b**) Anomalous difference Fourier maps for heavy atoms, derived from diffraction data measured from the native hSCD1 crystal (red mesh, contoured at 3σ) and from the SeMet-labeled crystal (blue mesh, contoured at 4σ). Blue mesh depicts the positions of two zinc ions and six selenium atoms. (**c**) The dimetal center in hSCD1. Zn1 is coordinated by five histidine residues, whereas Zn2 is coordinated by four histidine residues and a water molecule. The stearoyl-CoA substrate and zinc-coordinating histidine residues are shown in stick representation. Zincs and the water molecule are illustrated as black and blue spheres, respectively. Some residues in CH2 and loop regions are omitted for clarity. (**d**) Close-up view of zinc ion–binding sites. (**e**) Scheme of the hSCD1 active site. The two pro-*R* hydrogens (H_R) enclosed by dashed boxes are lost during dehydrogenation.

© 2015 Nature America, Inc. All rights reserved.

To gain more insight into the catalytic center of SCD1, we compared the dimetal center in hSCD1 with that in soluble Δ9 stearoyl-ACP desaturase from castor seed (PDB 1AFR)[4], which catalyzes the formation a *cis* double bond at the Δ9 position of stearic acid. We observed substantial differences between the two structures (**Supplementary Fig. 3a**,**b**). First, the dimetal center in hSCD1 is buried among TM2, CH2, TM4 and CH8, whereas in stearoyl-ACP desaturases the di-iron center is housed within a four-helix bundle[4]. Second, the metals in SCD1 are mainly coordinated by histidines in the histidine-box motifs (HXXXXH, HXXHH and HXXHH), but in stearoyl-ACP desaturase the irons are primarily ligated by residues with carboxylate groups (two EXXH motifs), to form a carboxylate-bridged di-iron center[4]. In fact, the four-helix bundle (a preferred scaffold for oxygen-activation mechanisms) and EXXH motifs are conserved in multiple di-iron center–containing enzymes[18], including acyl-ACP desaturase[7], multicomponent monooxygenase[18], epoxidase BoxB[19] (**Supplementary Fig. 3c**) and ribonucleotide redutase[20]. Altogether, the zinc-bound hSCD1 structure reveals a new di-metal center coordinated by a group of conserved histidine motifs.

Stearoyl-CoA–binding site

We identified prominent nonprotein electron density at the surface of the cytoplasmic cap domain and extending from the surface regions near CH2 and CH4 toward the cytoplasmic-facing C termini of TM2 and TM4 (**Fig. 3a**,**b**). The electron density feature was consistent with the substrate stearoyl-CoA, which serendipitously associated with hSCD1 during expression and remained bound throughout all phases of purification and crystallization.

The recognition of stearoyl-CoA by hSCD1 involves electrostatic and hydrophobic interactions (**Fig. 3** and **Supplementary Fig. 4a**). A large positively charged surface of SCD1 is adjacent to the negatively charged phosphates in the ADP group of CoA (**Fig. 3c**). The adenosine group of CoA mainly forms hydrogen-bond interactions with the side chains of residues Arg155 and Asp156 from CH2 and with the main chain carbonyl group of Gly197 (**Fig. 3d**,**e**). The side chain of Lys194 in CH4 forms a cation-π interaction with the adenine ring of CoA. The diphosphate groups form electrostatic interactions with the side chains of Arg188 and Lys189 in the loop between CH3 and CH4 (**Fig. 3e**). The pantothenate group interacts with side chains of Asn75 in TM1 and Asn148 in the loop between CH1 and CH2, by forming a hydrogen bond (**Fig. 3e**). The carbonyl group of the fatty acid forms a hydrogen bond with the indole group of Trp262 in TM4. The residues on SCD1 that form contacts with the stearoyl-CoA are also conserved in other isoforms in humans (hSCD5) and in the mouse SCD (**Supplementary Fig. 1**).

The acyl tail of the stearoyl-CoA inserts into a narrow hydrophobic tunnel lined by SCD1 residues Ala112, Ile115, Trp153, Val257, Ala260, Trp262, Val264 and Ala292 (**Fig. 3f**,**g**). The pronounced kink in the hydrophobic tunnel that holds the substrate (**Fig. 3f**) may be an important determinant that induces a *cis* conformation into the acyl chain of stearoyl-CoA. Furthermore, the length of the tunnel restrains carbons 9 and 10 of the acyl chain to align proximal to the relatively buried zincs that are bound to clusters of histidines inside the catalytic site of SCD1. The geometry of the hydrophobic cavity determines the regioselectivity of SCD1 for the *cis* dehydrogenation of the substrate.

To understand the determinants for regioselectivity, we compared the substrate-binding site of hSCD1 with the structure of BoxB[19], a di-iron–containing enzyme that dearomatizes a CoA-esterified benzoate (benzoyl-CoA) by epoxidation. The structure of BoxB (PDB 3PM5) shows a reduced iron center embedded in a canonical four-helix bundle with carboxylate-bridged coordination[19] (**Supplementary Fig. 3c**). Despite different configurations for metal binding in the catalytic centers of SCD1 and BoxB, we noticed that the substrate-protein interactions share striking similarities (**Supplementary Fig. 4**). First, stearoyl-CoA and benzoyl-CoA extend from the enzyme surfaces to the dimetal centers in both proteins, and the relevant catalytic groups (Δ9 position and phenyl ring in SCD1 and BoxB, respectively) are in proximity to the dimetal center. Second, the CoA groups in both systems interact with proteins by extensive electrostatic and hydrogen-bonding interactions (**Supplementary Fig. 4**). Notably, there is one polar group (Trp262 in SCD1 or Asn116 in BoxB) interacting with the thioester oxygen of the substrate (stearoyl-CoA

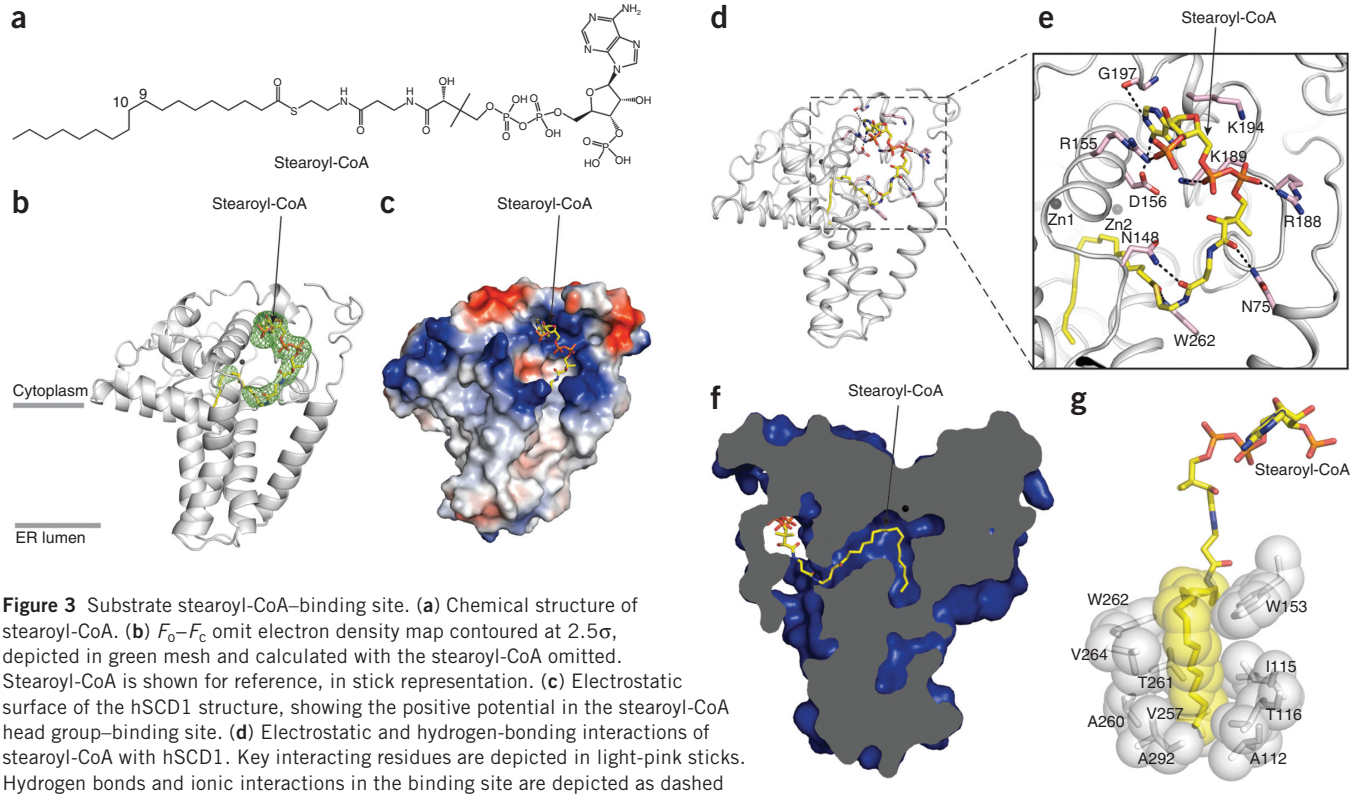

Figure 3 Substrate stearoyl-CoA–binding site. (**a**) Chemical structure of stearoyl-CoA. (**b**) F_o–F_c omit electron density map contoured at 2.5σ, depicted in green mesh and calculated with the stearoyl-CoA omitted. Stearoyl-CoA is shown for reference, in stick representation. (**c**) Electrostatic surface of the hSCD1 structure, showing the positive potential in the stearoyl-CoA head group–binding site. (**d**) Electrostatic and hydrogen-bonding interactions of stearoyl-CoA with hSCD1. Key interacting residues are depicted in light-pink sticks. Hydrogen bonds and ionic interactions in the binding site are depicted as dashed lines. (**e**) Close-up view of stearoyl-CoA–binding sites. (**f**) Cross-sections of the hSCD1 surface area (blue) showing a tunnel-like pocket for the acyl tail of stearoyl-CoA. The view of hSCD1 is rotated 180° anticlockwise in the membrane plane relative to the view in **Figure 3b–e**. (**g**) Hydrophobic interactions between stearoyl-CoA and hSCD1. Van der Waals surfaces for the acyl tail of substrate and interacting residues are shown as spheres. The view of hSCD1 is rotated 90° clockwise in the membrane plane relative to the view in **Figure 3b–e**.

© 2015 Nature America, Inc. All rights reserved.

or benzoyl-CoA) by a hydrogen bond (**Supplementary Fig. 4**). Such interactions contribute to determining the position of the acyl chain or phenyl ring. Third, the substrates adopt a kinked conformation after the thioester group in both structures, although the kink is much smaller in benzoyl-CoA than in stearoyl-CoA. Furthermore, both the stearoyl acid group in stearoyl-CoA and the benzoate group in benzoyl-CoA are accommodated by a hydrophobic pocket. In summary, the similarities in substrate-enzyme interactions featured in these two enzymes with different folding and functions help to highlight regioselectivity determinants in the CoA-containing dimetal enzymes.

DISCUSSION

The hSCD1 crystal structure provides a foundation for studying the determinants of regioselectivity and stereoselectivity in dehydrogenation by integral membrane dimetal desaturases. Because previous studies have indicated that the nature of the substrate head group determines the regioselectivity of desaurases[21], it seems likely that the CoA component contributes to the recognition step for the regioselective reaction in SCD1. This CoA-SCD1 interface involves the CoA groups (adenosine, diphosphate and pantothenate), which interact via hydrogen-bonding and electrostatic interactions with polar residues on the surface of SCD1. The binding site is further reinforced by the thioester oxygen of the fatty acid hydrogen-bonding with the indole group of the SCD1 surface-exposed residue Trp262. Presumably, once SCD1 engages the CoA head group of the substrate, then polar interactions guide the acyl chain of the fatty acid toward the hydrophobic tunnel between TM2 and TM4. In order for the acyl chain to fit into the tunnel, the bond between carbons 9 and 10 in the acyl chain of the substrate must adopt a *cis* conformation. The geometry of the lipophilic tunnel determines the regioselective *cis* dehydrogenation by SCD1. Furthermore, carbons 9 and 10 in the acyl chain align proximal to the dimetal center. The relative orientation between the dimetal center and the substrate (carbons 9 and 10) must allow for the pro-*R* dehydrogenation reaction. The final steps of the dehydration reaction presumably require additional factors (NADH, cytochrome b_5, cytochrome b_5 reductase and oxygen)[2] to dehydrogenate the pro-*R* hydrogens in carbons 9 and 10 via electron transfers. The structure of hSCD1 supports previous proposals[7] regarding regioselectivity and stereoselectivity in the mechanisms of dehydrogenation.

X-ray fluorescence and X-ray absorption spectroscopy experiments demonstrate that our hSCD1 crystals contain zinc ions. Although SCD1 is an iron-binding protein, we assigned zinc ions in the iron-binding site. It is not unusual to observe zinc ions bound in the iron-binding sites of metalloproteins. In fact the structure of recombinant quinodependent nitric oxide reductase (PDB 3AYF)[22] showed zincs in the nonheme metal–binding site, which is usually occupied by irons[23]. Although our SCD1 crystals contained zinc in the dimetal center of the enzyme, the structure nevertheless provides a valuable template for studying catalysis by the integral membrane SCD.

In summary, the hSCD1–substrate structure provides a molecular 'blueprint' for exploring the mechanism and pharmacology of SCD. To our knowledge, this is the first structure of a human integral membrane desaturase. The structure reveals a new histidine cluster for holding the dimetal center, which lies proximal to a prominent kink in the substrate-binding site within a long internal hydrophobic tunnel. The kink in the SCD1 internal tunnel presumably induces a *cis* conformation in the substrate and positions the substrate for desaturation by the dimetal center. Consistently with the well-known design

principle that 'form follows function', the SCD1 protein, with its internal kinked tunnel and metal center, has the ideal properties to control the point of desaturation. Future studies focused on elucidating biochemical and structural details of higher-ordered SCD1 complexes containing NADPH and cytochromes will enable better modeling of the enzymatic mechanisms of desaturation. This structure of isolated SCD1 yields new insights into the biochemical mechanisms of this important lipid-biosynthetic pathway and bolsters the framework for the optimization of SCD1 inhibitors to treat metabolic diseases and cancer.

METHODS

Methods and any associated references are available in the online version of the paper.

Accession codes. Coordinates and structure factors for hSCD1 have been deposited in the Protein Data Bank under accession code 4ZYO.

Note: Any Supplementary Information and Source Data files are available in the online version of the paper.

ACKNOWLEDGMENTS

We thank K. Wilson for critical comments. We thank the staff of the Berkeley Center for Structural Biology (BCSB) who operate ALS beamline 5.0.3 and the staff of GM/CA who operate APS beamline 23ID-D. The BCSB is supported in part by the US National Institutes of Health, US National Institute of General Medical Sciences, and GM/CA has been funded in whole or in part with federal funds from the US National Cancer Institute (Y1-CO-1020) and the US National Institute of General Medical Sciences (Y1-GM-1104). The Advanced Light Source and Advanced Photon Source are supported by the Director, Office of Science, Office of Basic Energy Sciences of the US Department of Energy, under contracts DE-AC02-05CH11231 and DE-AC02-06CH11357, respectively. Beamline 8.3.1 at the Advanced Light Source is operated by the University of California Office of the President, Multicampus Research Programs and Initiatives grant MR-15-328599 and Program for Breakthrough Biomedical Research, which is partially funded by the Sandler Foundation. Additional support comes from the US National Institutes of Health (GM105404, GM073210, GM082250 and GM094625), the US National Science Foundation (1330685), Plexxikon Inc. and the M.D. Anderson Cancer Center.

AUTHOR CONTRIBUTIONS

H.W. was responsible for research strategy; B.-C.S. designed the research and constructs; B.-C.S. and I.L. performed molecular biology; K.L. and H.Z. expressed native and SeMet-labeled protein, respectively; H.Z. purified both native and SeMet-labeled protein with input from H.W.; H.W. and M.G.K. performed crystallization; G.S. and W.L. collected and processed diffraction data and conducted X-ray fluorescence and absorption spectroscopy experiments; H.W. and M.G.K. determined the phases to solve the structure; H.W. built and refined the structure; and H.W. and M.G.K. analyzed the data and wrote the paper, incorporating comments from all authors.

COMPETING FINANCIAL INTERESTS

The authors declare no competing financial interests.

Reprints and permissions information is available online at http://www.nature.com/reprints/index.html.

1. Zhang, Z., Dales, N.A. & Winther, M.D. Opportunities and challenges in developing stearoyl-coenzyme A desaturase-1 inhibitors as novel therapeutics for human disease. *J. Med. Chem.* **57**, 5039–5056 (2014).
2. Enoch, H.G., Catala, A. & Strittmatter, P. Mechanism of rat liver microsomal stearyl-CoA desaturase: studies of the substrate specificity, enzyme-substrate interactions, and the function of lipid. *J. Biol. Chem.* **251**, 5095–5103 (1976).
3. Guy, J.E., Whittle, E., Kumaran, D., Lindqvist, Y. & Shanklin, J. The crystal structure of the ivy Δ4–16:0-ACP desaturase reveals structural details of the oxidized active site and potential determinants of regioselectivity. *J. Biol. Chem.* **282**, 19863–19871 (2007).
4. Lindqvist, Y., Huang, W., Schneider, G. & Shanklin, J. Crystal structure of delta9 stearoyl-acyl carrier protein desaturase from castor seed and its relationship to other di-iron proteins. *EMBO J.* **15**, 4081–4092 (1996).
5. Moche, M., Shanklin, J., Ghoshal, A. & Lindqvist, Y. Azide and acetate complexes plus two iron-depleted crystal structures of the di-iron enzyme Δ9 stearoyl-acyl carrier protein desaturase: implications for oxygen activation and catalytic intermediates. *J. Biol. Chem.* **278**, 25072–25080 (2003).
6. Whittle, E., Cahoon, E.B., Subrahmanyam, S. & Shanklin, J. A multifunctional acyl-acyl carrier protein desaturase from *Hedera helix* L. (English ivy) can synthesize 16- and 18-carbon monoene and diene products. *J. Biol. Chem.* **280**, 28169–28176 (2005).
7. Shanklin, J., Guy, J.E., Mishra, G. & Lindqvist, Y. Desaturases: emerging models for understanding functional diversification of diiron-containing enzymes. *J. Biol. Chem.* **284**, 18559–18563 (2009).
8. Man, W.C., Miyazaki, M., Chu, K. & Ntambi, J.M. Membrane topology of mouse stearoyl-CoA desaturase 1. *J. Biol. Chem.* **281**, 1251–1260 (2006).
9. Stefan, N. *et al.* Low hepatic stearoyl-CoA desaturase 1 activity is associated with fatty liver and insulin resistance in obese humans. *Diabetologia* **51**, 648–656 (2008).
10. Morgan-Lappe, S.E. *et al.* Identification of Ras-related nuclear protein, targeting protein for *Xenopus* kinesin-like protein 2, and stearoyl-CoA desaturase 1 as promising cancer targets from an RNAi-based screen. *Cancer Res.* **67**, 4390–4398 (2007).
11. Dobrzyn, A. & Ntambi, J.M. Stearoyl-CoA desaturase as a new drug target for obesity treatment. *Obes. Rev.* **6**, 169–174 (2005).
12. Igal, R.A. Roles of stearoylCoA desaturase-1 in the regulation of cancer cell growth, survival and tumorigenesis. *Cancers* (*Basel*) **3**, 2462–2477 (2011).
13. Attie, A.D. *et al.* Relationship between stearoyl-CoA desaturase activity and plasma triglycerides in human and mouse hypertriglyceridemia. *J. Lipid Res.* **43**, 1899–1907 (2002).
14. Hulver, M.W. *et al.* Elevated stearoyl-CoA desaturase-1 expression in skeletal muscle contributes to abnormal fatty acid partitioning in obese humans. *Cell Metab.* **2**, 251–261 (2005).
15. Liu, G. Stearoyl-CoA desaturase inhibitors: update on patented compounds. *Expert. Opin. Ther. Pat.* **19**, 1169–1191 (2009).
16. Powell, D.A. An overview of patented small molecule stearoyl coenzyme-A desaturase inhibitors (2009–2013). *Expert. Opin. Ther. Pat.* **24**, 155–175 (2014).
17. Shanklin, J., Whittle, E. & Fox, B.G. Eight histidine residues are catalytically essential in a membrane-associated iron enzyme, stearoyl-CoA desaturase, and are conserved in alkane hydroxylase and xylene monooxygenase. *Biochemistry* **33**, 12787–12794 (1994).
18. Sazinsky, M.H. & Lippard, S.J. Correlating structure with function in bacterial multicomponent monooxygenases and related diiron proteins. *Acc. Chem. Res.* **39**, 558–566 (2006).
19. Rather, L.J. *et al.* Structure and mechanism of the diiron benzoyl-coenzyme A epoxidase BoxB. *J. Biol. Chem.* **286**, 29241–29248 (2011).
20. Nordlund, P., Sjöberg, B.M. & Eklund, H. Three-dimensional structure of the free radical protein of ribonucleotide reductase. *Nature* **345**, 593–598 (1990).
21. Heilmann, I., Mekhedov, S., King, B., Browse, J. & Shanklin, J. Identification of the *Arabidopsis* palmitoyl-monogalactosyldiacylglycerol delta7-desaturase gene FAD5, and effects of plastidial retargeting of *Arabidopsis* desaturases on the fad5 mutant phenotype. *Plant Physiol.* **136**, 4237–4245 (2004).
22. Matsumoto, Y. *et al.* Crystal structure of quinol-dependent nitric oxide reductase from *Geobacillus stearothermophilus*. *Nat. Struct. Mol. Biol.* **19**, 238–245 (2012).
23. Hino, T. *et al.* Structural basis of biological N_2O generation by bacterial nitric oxide reductase. *Science* **330**, 1666–1670 (2010).

© 2015 Nature America, Inc. All rights reserved.

ONLINE METHODS

Construct protein expression, purification and crystallization. The hSCD1 crystallization construct contains cDNA encoding the human SCD1 protein (GenBank AAH62303.1). To improve crystallization behavior, 45 amino acid residues were removed from the N terminus of the polypeptide, and three surface mutations (K60A, K62A and E63A) were introduced[24]. The cDNA encoding SCD1 was cloned in frame behind an N-terminal hexahistidine tag that was engineered with a TEV protease–cleavage site. Recombinant baculovirus was generated and amplified in Sf9 cells (Invitrogen). Cells were typically harvested 66 h after viral infection. For SeMet labeling, Sf9 cells were cultured in methionine-free medium (Expression Systems) for 16 h before infection with recombinant baculovirus and addition of 70 mg l^{-1} SeMet (Molecular Dimensions). Membranes were extracted from the cell pellets with standard methods.

The harvested membrane was solubilized by 25 mM Tris, pH 7.6, 800 mM NaCl, 20 mM imidazole, 0.25 mM TCEP, 1% (w/v) *n*-dodecyl-β-D-maltoside (DDM, Anatrace) and EDTA-free protease inhibitors. Upon solubilization, the hSCD1 was purified by Ni-NTA Superflow resin (Qiagen) and eluted by 25 mM Tris, pH 7.6, 200 mM NaCl, 5% glycerol, 0.025% (w/v) DDM, 0.25 mM TCEP and 250 mM imidazole. After cleavage of the hexahistidine tag by TEV protease, hSCD1 was desalted by PD-10 column (GE Healthcare) and further purified by Ni-NTA Superflow column. Finally, hSCD1 was applied to a size-exclusion chromatography column (Superdex 200, 10/300 GL, GE Healthcare) in buffer containing 25 mM Tris, pH 7.2, 200 mM NaCl, 1 mM TCEP and 0.02% (w/v) octaethylene glycol monododecyl ether ($C_{12}E_8$, Anatrace). The peak fractions were collected and concentrated to 8.5 mg ml^{-1} before crystallization.

Both native and SeMet-labeled hSCD1 were crystallized by vapor diffusion at 4 °C with the crystallization reservoir solution containing 100 mM Tris-HCl, pH 8.5, 30–35% (v/v) PEG 400 and 220 mM sodium citrate. For phasing purposes, the native crystals were soaked in 1 mM hexatantalum tetradecabromide (Ta_6Br_{12}) overnight before being frozen in liquid nitrogen.

Data collection and structure elucidation. X-ray fluorescence spectroscopy experiments were performed at beamline 8.3.1 of the Advanced Light Source on native SCD1 crystals. The crystallization solution was removed from the loop containing the crystals to reduce its influence on the measurements.

Diffraction data sets were collected at the Advanced Photon Source (Argonne National Laboratory, beamline 23ID-D) and the Advanced Light Source (beamline 5.0.3). For Ta_6Br_{12}-soaked and SeMet-labeled crystals, data were collected at the L_{II} edge (1.11 Å) of tantalum and at the K edge of selenium (0.979 Å), respectively. Data sets were indexed, integrated and scaled with HKL2000 software[25].

The initial phases for the hSCD1 structure were calculated from anomalous signal in a data set from a crystal soaked with Ta_6Br_{12}, by SAD[26]. Two sites for the heavy metals were determined by hybrid substructure search (HySS) in Phenix[27]. Heavy atom sites were refined with AutoSol implemented in Phenix[27], which generated an experimentally phased map (map I) that contained clear solvent boundaries and obvious features consistent with the TM helices. We later realized that the two metals identified from Ta_6Br_{12}-soaked crystals are not tantalum clusters but rather are the two intrinsic zinc ions. To complete the structure, we collected anomalous data from multiple SeMet-labeled hSCD1 crystals. The selenium sites were manually positioned with anomalous difference Fourier maps calculated from phases from the zinc ions, as described above. The highest-resolution selenium data set contained eight heavy atoms (six selenium and two zinc); these sites were refined in AutoSol in Phenix[27] for SAD phasing, to yield the second density map (map II). The hSCD1 model was built in Coot[28] on the basis of both map I and map II. Refinement of the model against the X-ray data in Phenix[27] was carried out until satisfactory model statistics were obtained. The final model contains residues 53–350 of hSCD1, a stearoyl-CoA molecule, two zinc ions, a detergent molecule and a water molecule. Regions with weak electron density were excluded in the final model.

The structure quality analysis was carried out with MolProbity[29]. For the final structure, the Ramachandran geometry is excellent, with 90% of the residues in the most favored regions and none in disallowed regions. The anomalous difference maps were calculated with the fast Fourier transform in the CCP4 suite[30]. All structure figures were generated with PyMOL (http://www.pymol.org/).

Sequence alignment. Multiple sequence alignments were performed with Clustal Omega[31] and were edited in Jalview[32].

24. Derewenda, Z.S. Rational protein crystallization by mutational surface engineering. *Structure* **12**, 529–535 (2004).
25. Otwinowski, Z. & Minor, W. Processing of X-ray diffraction data collected in oscillation mode. *Methods Enzymol.* **276**, 307–326 (1997).
26. Wang, B.C. Resolution of phase ambiguity in macromolecular crystallography. *Methods Enzymol.* **115**, 90–112 (1985).
27. Adams, P.D. *et al.* Phenix: a comprehensive python-based system for macromolecular structure solution. *Acta Crystallogr. D Biol. Crystallogr.* **66**, 213–221 (2010).
28. Emsley, P. & Cowtan, K. Coot: model-building tools for molecular graphics. *Acta Crystallogr. D Biol. Crystallogr.* **60**, 2126–2132 (2004).
29. Chen, V.B. *et al.* Molprobity: all-atom structure validation for macromolecular crystallography. *Acta Crystallogr. D Biol. Crystallogr.* **66**, 12–21 (2010).
30. Collaborative Computing Project. The CCP4 suite: programs for protein crystallography. *Acta Crystallogr. D Biol. Crystallogr.* **50**, 760–763 (1994).
31. Sievers, F. *et al.* Fast, scalable generation of high-quality protein multiple sequence alignments using Clustal Omega. *Mol. Syst. Biol.* **7**, 539 (2011).
32. Waterhouse, A.M., Procter, J.B., Martin, D.M.A., Clamp, M. & Barton, G.J. Jalview Version 2: a multiple sequence alignment editor and analysis workbench. *Bioinformatics* **25**, 1189–1191 (2009).

© 2015 Nature America, Inc. All rights reserved.

doi:10.1038/nsmb.3049